Nanoscale

COMMUNICATION

View Article Online
View Journal | View Issue

Cite this: *Nanoscale*, 2017, **9**, 3747

Received 25th August 2016,
Accepted 10th February 2017

DOI: 10.1039/c6nr06740a

rsc.li/nanoscale

Binary halide, ternary perovskite-like, and perovskite-derivative nanostructures: hot injection synthesis and optical and photocatalytic properties†

Suh-Ciuan Lim,‡[a] Hsuan-Peng Lin,‡[a] Wei-Lun Tsai,[b] Hao-Wu Lin,[b] Yao-Tsung Hsu[a] and Hsing-Yu Tuan*[a]

A variety of crystalline colloid binary halide, ternary perovskite-like and ternary perovskite-derivative nanostructures with well-defined morphologies were synthesized, thus expanding materials chemistry to the new category of nanomaterials. The optical and photocatalytic properties of ternary nanostructures were investigated.

In recent years, materials such as alkali halides, perovskite-like and perovskite derivatives have attracted more significant attention due to their optical or photovoltaic characteristics. An alkali halide thin film layer can be applied as a heavily doped semiconductor due to its metallic transport characteristics.[1–5] Perovskite compounds of ABX_3 structure share a BX_6 octahedron on each side, where the A (K, Rb or Cs) cation can balance the charge to achieve electrical neutrality, the B atom is a metal cation (Pb^{2+} or Sn^{2+}) and X refers to Cl^-, Br^- and I^-. Perovskites have been widely applied in light-emitting diodes, lasers and photoelectric conversion devices, thus they can efficiently replace the dyes in dye-sensitized solar cells (DSSC) with yield efficiencies close to 20%.[6–10] Recently, perovskite nanomaterials have attracted attention owing to their stable material platforms that are applicable in tunable lasers and other nanoscale optoelectronic devices.[11–13] Perovskite-like APb_2Cl_5 materials (A = K or Rb), where Pb^{2+} is the same as in the perovskite structure, are also a potential candidate to be applied in dye-sensitized solar cells and can be used in many mid-IR applications, such as pollution monitoring and medical diagnostics.[14–17] On the other hand, perovskite derivatives (a new type of perovskite) A_2SnCl_6 (A = Rb or Cl), where Sn is at the 4^+ oxidation state, have an octahedral structure that can make it remain more stable and anti-moisture in the atmosphere. They can be applied as hole-transporting materials (HTMs) in DSSC that improve the performance of photovoltaic devices.[18–20] Binary alkali halides exist as mineral salts in nature and can be applied as thin films for electronic sensing devices.[21]

Binary, perovskite-like and perovskite-derivative thin films or bulk materials normally can be obtained by thin film deposition, high temperature annealing, ball milling, wet chemical etching, and the co-precipitation method.[21–26] However, there are only a few cases reporting the synthesis of nanoscale alkali halide, perovskite-like and perovskite derivative nanomaterials: only two examples about the synthesis of nanometer scale halides: LiF and NaCl;[27,28] two examples for perovskite-like KSn_2F_5 and $CsPb_2Br_5$;[29,30] no examples for perovskite derivatives. Thus, it is still necessary to synthesize halides or perovskite related materials in view of fundamental research and other applications.

In this study, we report a general approach to obtain crystalline binary halide, ternary perovskite-like and ternary perovskite-derivative nanostructures with a variety of morphologies including octahedra, nanowires, spheres, cubes, polyhedra and nanorods *via* a hot injection and heating up synthesis using various halide precursor compounds. The reducing agents or surfactants applied included oleylamine (OLA), trioctylphosphine (TOP), *N*-methyl-2-pyrrolidone (NMP) and oleic acid (OA). Finally, the optical and photocatalytic properties of perovskite-like and perovskite derivative nanomaterials were evaluated. Fig. 1 shows the scheme of colloid synthesis of various alkali metal binary or ternary halides. Simply, the degassed and pre-heated alkali metal oleate solution was injected into a solution with ligands or reducing agents under an inert gas atmosphere at a certain temperature, which was varied to totally dissolve of the halide salt precursors and the mixture was then heated up to reaction temperature. This strategy has successfully produced zero-dimensional (0D) nanoparticles of various shapes with well-defined morphologies,

[a]*Department of Chemical Engineering, National Tsing Hua University, 101, Section 2, Kuang-Fu Road, Hsinchu, Taiwan 30013, Republic of China. E-mail: hytuan@che.nthu.edu.tw*
[b]*Department of Materials Science and Engineering, National Tsing Hua University, 101, Section 2, Kuang-Fu Road, Hsinchu, Taiwan 30013, Republic of China*

†Electronic supplementary information (ESI) available: Detailed Experimental section, low resolution SEM images of as-synthesised nanomaterials and UV-vis spectra recorded during the photocatalytic degradation of Rh6G using different samples. See DOI: 10.1039/c6nr06740a

‡These authors contributed equally to this work.

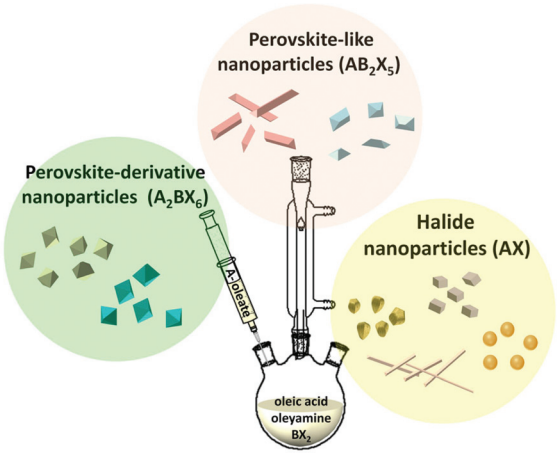

Fig. 1 Schematic illustrating the colloid synthesis process for different binary halide nanoparticles AX (A = K, Rb, Cs and X = Cl, Br, I), ternary perovskite-like nanoparticles APb_2Cl_5 (A = K, Rb), and ternary perovskite-derivative nanoparticles A_2SnCl_5, (A = Rb, Cs) mediated by oleic acid and oleylamine as ligands or reducing agents.

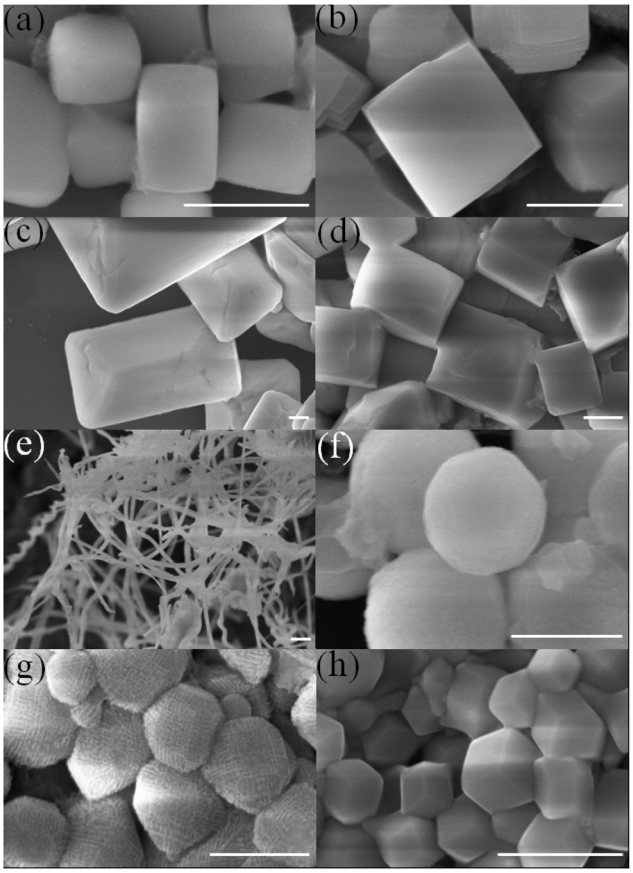

Fig. 2 Representative SEM micrographs of binary halide nanoparticles: (a) KCl, (b) KBr, (c) RbCl, (d) RbBr, (e) RbI, (f) CsCl, (g) CsBr, (h) CsI. Scale bar, 500 nm.

including cubes, cuboids, wire-like, yarn ball-like, spheres, short rods, and octahedra (for the Experimental section, characterization and measurement details, see ESI and Table S1, ESI†). The morphologies of as-synthesized binary alkali halides are shown in Fig. 2. The average diameters or lengths of most of the nanocrystals were measured to be 300–500 nm and ~800 nm. However, the RbCl and RbBr crystals were larger, on a submicron scale with an average length of 1–2 μm. The corresponding low resolution SEM images demonstrated the uniform distribution and mass production of the halide nanocrystals (Fig. S1, ESI†). Most of the nanoparticles or crystals were cuboids or cube shapes. The CsI crystals have the most special morphology; they look like yarn balls which were wrapped layer by layer, thus RbI halides have grown into a wire-like shape and CsI crystals were the sole sphere shape among all. The corresponding XRD patterns of all binary halide samples obtained are shown in Fig. 3. In all the XRD patterns, we can observe that almost all the experimental results are in agreement with the binary halides of the Joint Committee on Powder Diffraction Standards (JCPDS) cards, except CsCl, which shows 2 extra peaks. These peaks could have resulted from the residual in the precursor materials that required a higher temperature or a stronger reducing agent for its removal.

Based on the concept of synthesis of binary halides (including KCl, RbCl, CsCl) at the submicron or nano scale, we further extended it to obtain ternary perovskite-like or perovskite-derivative nanomaterials. Expectedly, we successfully obtained 4 ternary compounds in the nano scale, namely KPb_2Cl_5, $RbPb_2Cl_5$, Rb_2SnCl_6 and Cs_2SnCl_6. To synthesize perovskite-like (APb_2Cl_5 (A = K, Rb)) and perovskite-derivative (A_2SnCl_6 (A = Rb, Cs)) nanoparticles, alkali metal oleate solutions were prepared by mixing X_2CO_3 (X = K, RB, Rb, Cs) with ODE and OA at 180 °C. Ternary nanoparticles were synthesized by reacting an alkali metal oleate solution and a $PbCl_2$ or $SnCl_2$ solution at 220–240 °C for around 30 min (see the ESI† for details). The as-synthesized nanomaterials were first studied by scanning electron microscopy (SEM) for their morphology and structure, and the results are shown in Fig. 4. Also, the low resolution SEM images have provided evidence of the mass production and uniform shapes of the perovskite-likes and perovskite derivatives (Fig. S2, ESI†). The morphology of the two perovskite-like compounds APb_2Cl_5 (A = K, Rb) is a rod or short rod shape with the size of the crystals being about 100–500 nm. On the other hand, the morphology of two perovskite-like compounds APb_2Cl_5 (A = K, Rb) is a rod or short rod shape with the size of the crystals being about 100–500 nm. On the other hand, the A_2SnCl_6 compounds (A = Rb, Cs) looked similar as well; both of them are octahedral with edge length measured to be 400–500 nm. It is possible that the octahedral-like shape was decided by a certain orientation or elongation direction of the component atoms in the crystal structure. This phenomenon is in good agreement with the previous case of a reported Sn-deficient perovskite derivative Cs_2SnI_6, consisting of isolated SnI_6^{4-} octahedra.[24] Interestingly, the Cs_2SnCl_6 crystals can form two other shapes: plate-like and whisker-like by replacing the surfactant or

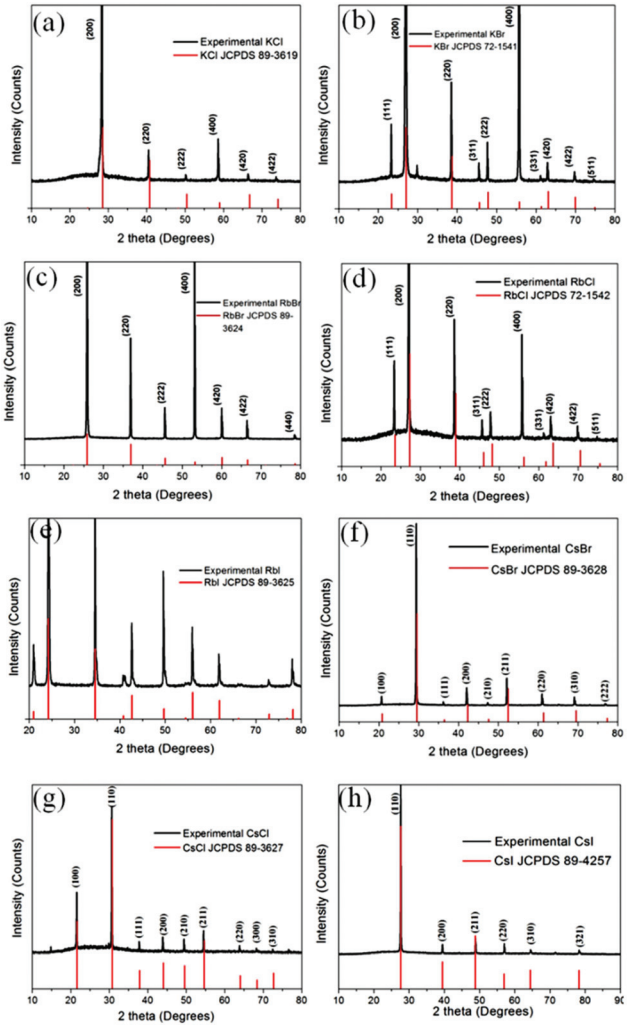

Fig. 3 X-ray diffraction patterns of binary halide nanoparticles: (a) KCl, (b) KBr, (c) RbCl, (d) RbBr, (e) RbI, (f) CsCl, (g) CsBr, (h) CsI.

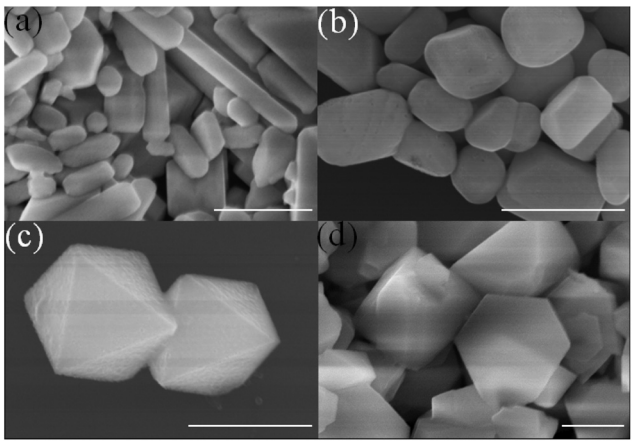

Fig. 4 Representative SEM micrographs of ternary perovskite-like nanoparticles: (a) KPb_2Cl_5, (b) $RbPb_2Cl_5$ and ternary perovskite-derivative nanoparticles (c) Rb_2SnCl_6, (d) Cs_2SnCl_6. Scale bar, 500 nm.

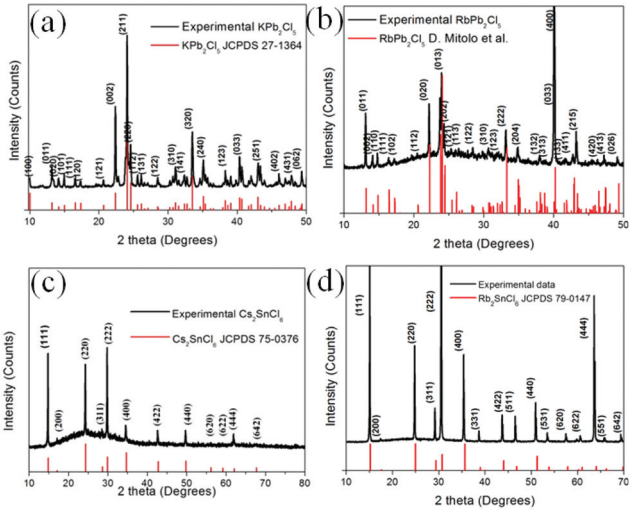

Fig. 5 X-ray diffraction patterns of ternary perovskite-like nanoparticles: (a) KPb_2Cl_5, (b) $RbPb_2Cl_5$ and ternary perovskite-derivative nanoparticles: (c) Rb_2SnCl_6, (d) Cs_2SnCl_6.

reducing agent OLA with TOP and performing fine adjustments of the reaction temperature (Fig. S3 and Table S1, ESI†). The corresponding XRD patterns of all ternary perovskite-like and perovskite-derivative nanoparticles obtained are shown in Fig. 5. In all these patterns, almost all the experimental results were in good agreement with the previously reported JCPDS cards or ternary halide case ($RbPb_2Cl_5$).[31]

The above ternary alkali metal halides were then analysed by transmission electron microscopy (TEM) and the corresponding results are shown in Fig. 6. The SAED analysis was also performed on a typical individual crystal of the samples. The central spot in the diffraction pattern in Fig. 6c, f and h represents the single crystalline structure with the crystallographic orientation [0 1 0] for KPb_2Cl_5, [0 −3 1] for $RbPb_2Cl_5$ and [1 1 1] for Rb_2SnCl_6. Both KPb_2Cl_5 and $RbPb_2Cl_5$ nanorods grow along the [100] crystal planes. The other spots representing [2 −2 0], [0 −2 2], [2 0 −2] are also marked in the SAED pattern of Rb_2SnCl_6. The microstructure information of KPb_2Cl_5 and $RbPb_2Cl_5$ nanorods was further characterized by HRTEM. The lattice spacing was calculated from the lattice structure of $RbPb_2Cl_5$ (Fig. 6b); lattice dots were aligned in intervals of 3.12 Å in the longer directional axis of the short rod crystal and in intervals of 2.21 Å at the perpendicular direction to the longer directional axis. These intervals with distances of 3.12 Å and 2.21 Å correlate to the distances of (004) and (400) at KPb_2Cl_5, which has a monoclinic crystal structure with $P2_1/c$ space group that is in agreement with JCPDS card no. 27-1364. Interestingly, we found that the $RbPb_2Cl_5$ crystal has the same atomic positions or coordinates but different lattice parameters than the KPb_2Cl_5 crystal. The lattice spacing analysis by HRTEM of a single $RbPb_2Cl_5$ nanorod (Fig. 6e) has shown its similarity of crystal structure to KPb_2Cl_5, which is also a group member of monoclinic $P2_1/c$ space group.[24] Its lattice dots were aligned in intervals of 8.96 Å in the longer

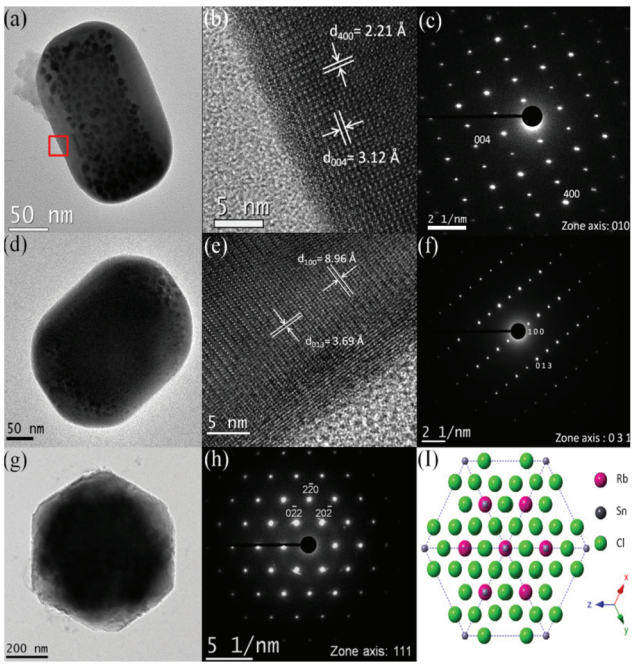

Fig. 6 Structural characterization of ternary perovskite-like nanoparticles and ternary perovskite-derivative nanoparticles. (a) Representative TEM image of perovskite-like nanoparticles KPb_2Cl_5 and (b–c) the corresponding SAED pattern and HRTEM analyses. (d) Representative TEM image of perovskite-like nanoparticles $RbPb_2Cl_5$ and (e–f) the corresponding SAED pattern and HRTEM analyses. (g) Representative TEM image of ternary perovskite-derivative nanoparticles Rb_2SnCl_6 and the corresponding SAED patterns (h); schematic illustrating the atomic structure (i), showing their single-crystalline structures.

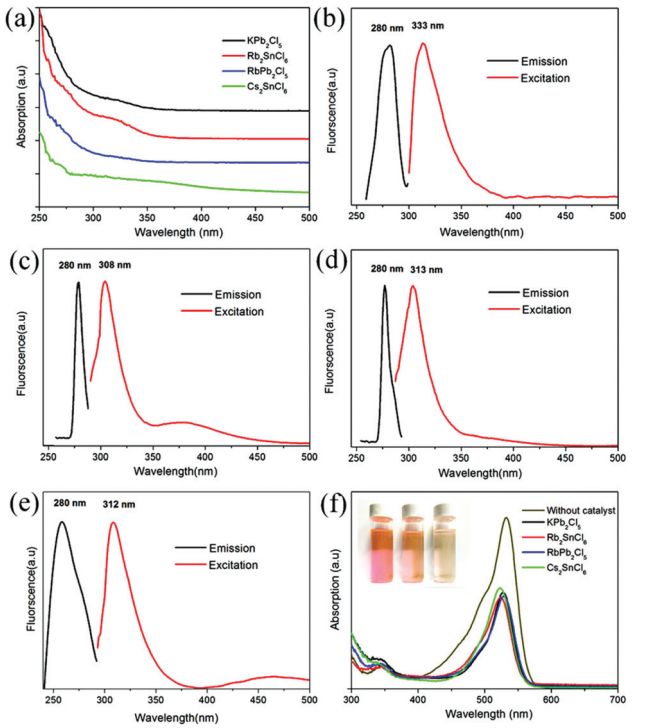

Fig. 7 (a) UV-vis spectra of ternary perovskite-like or perovskite-derivative nanoparticles. PL excitation and emission spectra of (b) KPb_2Cl_5, (c) Rb_2SnCl_6, (d) $RbPb_2Cl_5$, (e) Cs_2SnCl_6. (f) UV-vis spectra recorded during the photocatalytic degradation of Rh6G by using different catalysts. The reaction time for all curves is 2 h for the convenience of comparison. The inset demonstrates the color change after adding KPb_2Cl_5 for 0 h, 1 h and 3 h, from left to right respectively.

directional axis of the short rod crystal and in intervals of 3.69 Å at the perpendicular direction to the longer directional axis. The interplanar spacings of 8.96 Å and 3.69 Å were corresponding to the (100) and (013) planes of the $RbPb_2Cl_5$ crystal structure.

Fig. 7 shows the representative spectra of UV-vis absorption, PL excitation and emission profiles, and photocatalytic activities of the as-synthesized perovskite-like and perovskite-derivative nanomaterials dispersed in a tetrahydrofuran (THF) solution (for characterization and measurement details see the ESI†). As shown in Fig. 7a, all the perovskite-like or perovskite-derivative nanocrystals begin to increase in their intensity of peaks from around 280 nm and show strong absorbance in the range of deep UV (<250 nm). It is remarkable that deep UV-emitting materials have very rarely been reported,[32–34] and there is not any example reported about UV-emitting perovskite-derivative or perovskite-like nanomaterials. Fig. 7b–e shows PL excitation and emission spectra of KPb_2Cl_5 (b), Rb_2SnCl_6 (c), $RbPb_2Cl_5$ (d), and Cs_2SnCl_6 (e). All the PL excitation spectra show excitation peaks centered at about 280 nm, which are consistent with the features of the absorption spectra in Fig. 7a. The emission peak was found at 333 nm for KPb_2Cl_5, 308 nm for Rb_2SnCl_6, 313 nm for $RbPb_2Cl_5$, and 312 nm for Cs_2SnCl_6. The photocatalytic activities of the as-synthesized perovskite-like and perovskite-derivative nanomaterials were evaluated by decomposing rhodamine 6G (Rh6G) in THF solutions under UV irradiation. Fig. 7f shows the absorption profiles of Rh6G during the photocatalytic process (for photocatalytic testing details see the ESI†). All the irradiation times are kept at 2 h for comparison. The sample without adding any catalysts has the strongest absorption peak centered at about 530 nm. For perovskite-like nanocrystals (Fig. S4a and c, ESI†), the concentration of Rh6G is reduced by about 42% after 2 h and 60% after 3 h of UV irradiation, while the concentrations of Rh6G for the perovskite-derivative nanocrystals (Fig. S4b and d, ESI†) were reduced by about 39% after 2 h and 47% after 3 h of UV irradiation. By comparing the photocatalytic activities of the four different perovskite related nanocrystals, from the highest to the lowest in rank, they are in the order: $RbPb_2Cl_5$, KPb_2Cl_5, Rb_2SnCl_6 and Cs_2SnCl_6.

Conclusions

In summary, we report a facile colloid-phase approach for the synthesis of binary halide, ternary perovskite-like and perovskite-derivative nanocrystals: 8 types of binary halides, including KCl, KBr, RbCl, RbBr, RbI, CsCl, CsBr, and CsI, 2 types of

perovskite-like nanomaterials: KPb_2Cl_5, $RbPb_2Cl_5$, and 2 types of perovskite-derivatives: Rb_2SnCl_6, Cs_2SnCl_6. All of these nanomaterial syntheses are reported for the first time. It was considered that the binary halide system, namely AX (A = Li, Na, K, Rb, Cs and X = F, Cl, Br, I), exists as 20 types of binary compounds. The ternary perovskite related system, perovskite-like AB_2X_5 (B = Si, Ge, Sn, Pb) and perovskite-derivative A_2BX_6 could respectively form 80 types of ternary compounds. It is believed that the reported synthesis can be applied to up to 180 combinations of halides or perovskite-related nanomaterials, which is critical for expanding materials chemistry to the new category of nanomaterials. Interestingly, the absorption and luminescence spectra of KPb_2Cl_5, $RbPb_2Cl_5$, Cs_2SnCl_6, and Rb_2SnCl_6 are located in the ultraviolet region. This is a fascinating result as most of the perovskite related materials absorb or emit infrared and visible light.[7,35,36] All in all, controlled synthesis of perovskite-like and perovskite-derivative nanocrystals featuring the characteristic of energetically-derived photoluminescence, is highly valuable for further research to promote the development of electronic and photovoltaic devices.

Notes and references

1 A. Lushchik, E. Feldbach, R. Kink, C. Lushchik, M. Kirm and I. Martinson, *Phys. Rev. B: Condens. Matter*, 1996, **53**, 5379–5387.
2 R. Webster, L. Bernasconi and N. M. Harrison, *J. Chem. Phys.*, 2015, 142.
3 B. F. Bory, J. X. Wang, H. L. Gomes, R. A. J. Janssen, D. M. De Leeuw and S. C. J. Meskers, *Appl. Phys. Lett.*, 2014, 105.
4 J. Liu, X. H. Zhang, G. J. Sun, B. Wang, T. C. Zhang, F. T. Yi and P. Liu, *Mater. Sci. Semicond. Process.*, 2015, **40**, 44–49.
5 Y. S. Cohen, Y. Gabay and Y. Cohen, *ECS Electrochem. Lett.*, 2015, **4**, H1–H4.
6 H. M. Zhu, Y. P. Fu, F. Meng, X. X. Wu, Z. Z. Gong, Q. Ding, M. V. Gustafsson, M. T. Trinh, S. Jin and X. Y. Zhu, *Nat. Mater.*, 2015, **14**, 636–U115.
7 L. Protesescu, S. Yakunin, M. I. Bodnarchuk, F. Krieg, R. Caputo, C. H. Hendon, R. X. Yang, A. Walsh and M. V. Kovalenko, *Nano Lett.*, 2015, **15**, 3692–3696.
8 D. D. Zhang, S. W. Eaton, Y. Yu, L. T. Dou and P. D. Yang, *J. Am. Chem. Soc.*, 2015, **137**, 9230–9233.
9 K. F. Wu, G. J. Liang, Q. Y. Shane, Y. P. Ren, D. G. Kong and T. Q. Lian, *J. Am. Chem. Soc.*, 2015, **137**, 12792–12795.
10 O. Vybornyi, S. Yakunin and M. V. Kovalenko, *Nanoscale*, 2016, **8**, 6278–6283.
11 S. Yakunin, L. Protesescu, F. Krieg, M. I. Bodnarchuk, G. Nedelcu, M. Humer, G. De Luca, M. Fiebig, W. Heiss and M. V. Kovalenko, *Nat. Commun.*, 2015, **6**, 8056.
12 S. W. Eaton, M. L. Lai, N. A. Gibson, A. B. Wong, L. T. Dou, J. Ma, L. W. Wang, S. R. Leone and P. D. Yang, *Proc. Natl. Acad. Sci. U. S. A.*, 2016, **113**, 1993–1998.
13 Y. P. Fu, H. M. Zhu, C. C. Stoumpos, Q. Ding, J. Wang, M. G. Kanatzidis, X. Y. Zhu and S. Jin, *ACS Nano*, 2016, **10**, 7963–7972.
14 I. N. Ogorodnikov, N. S. Bastrikova, V. A. Pustovarov and L. I. Isaenko, *J. Opt. Soc. Am. B*, 2014, **31**, 1935–1941.
15 R. Balda, M. Voda, M. Al-Saleh and J. Fernandez, *J. Lumin.*, 2002, **97**, 190–197.
16 S. V. Mel'nikova, L. I. Isaenko, V. M. Pashkov and I. V. Pevnev, *Phys. Solid State*, 2006, **48**, 2152–2156.
17 O. N. Yunakova, V. K. Miloslavksy, E. N. Kovalenko and V. V. Kovalenko, *Low Temp. Phys.*, 2015, **41**, 645–648.
18 B. Lee, C. C. Stoumpos, N. Zhou, F. Hao, C. Malliakas, C. Y. Yeh, T. J. Marks, M. G. Kanatzidis and R. P. Chang, *J. Am. Chem. Soc.*, 2014, **136**, 15379–15385.
19 H. Donker, W. M. A. Smit and G. Blasse, *J. Phys. Chem. Solids*, 1989, **50**, 603–609.
20 A. Kaltzoglou, M. Antoniadou, A. G. Kontos, C. C. Stoumpos, D. Perganti, E. Siranidi, V. Raptis, K. Trohidou, V. Psycharis, M. G. Kanatzidis and P. Falaras, *J. Phys. Chem. C*, 2016, **120**, 11777–11785.
21 I. Beinik, C. Barth, M. Hanbucken and L. Masson, *Sci. Rep.*, 2015, 5.
22 R. Kral, K. Nitsch, V. Babin, J. Sulc, H. Jelinkova, Y. Yokota, A. Yoshikawa and M. Nikl, *Opt. Mater.*, 2013, **36**, 214–220.
23 R. Kral, *J. Cryst. Growth*, 2012, **360**, 162–166.
24 B. Saparov, J. P. Sun, W. W. Meng, Z. W. Xiao, H. S. Duan, O. Gunawan, D. Shin, I. G. Hill, Y. F. Yan and D. B. Mitzi, *Chem. Mater.*, 2016, **28**, 2315–2322.
25 L. N. Patro and K. Hariharan, *Ionics*, 2013, **19**, 643–649.
26 A. Katelnikovas, J. Plewa, S. Sakirzanovas, D. Dutczak, D. Enseling, F. Baur, H. Winkler, A. Kareiva and T. Justel, *J. Mater. Chem.*, 2012, **22**, 22126–22134.
27 B. B. Wang, P. Jin, Y. Z. Yue, S. D. Ji, Y. M. Li and H. J. Luo, *RSC Adv.*, 2015, **5**, 5072–5076.
28 C. B. Jiang, B. Wu, Z. Q. Zhang, L. Lu, S. X. Li and S. X. Mao, *Appl. Phys. Lett.*, 2006, 88.
29 K. H. Wang, L. Wu, L. Li, H. B. Yao, H. S. Qian and S. H. Yu, *Angew. Chem., Int. Ed.*, 2016, **55**, 8328–8332.
30 L. N. Patro and K. Hariharan, *Mater. Res. Bull.*, 2012, **47**, 2492–2497.
31 D. Mitolo, D. Pinto, A. Garavelli, L. Bindi and F. Vurro, *Mineral. Petrol.*, 2009, **96**, 121–128.
32 N. Nepal, J. M. Zavada, D. S. Lee, A. J. Steckl, A. Sedhain, J. Y. Lin and H. X. Jiang, *Appl. Phys. Lett.*, 2009, 94.
33 L. B. Tang, R. B. Ji, X. K. Cao, J. Y. Lin, H. X. Jiang, X. M. Li, K. S. Teng, C. M. Luk, S. J. Zeng, J. H. Hao and S. P. Lau, *ACS Nano*, 2012, **6**, 5102–5110.
34 Y. Y. Liu and D. Y. Kim, *Chem. Commun.*, 2015, **51**, 4176–4179.
35 E. R. Dohner, A. Jaffe, L. R. Bradshaw and H. I. Karunadasa, *J. Am. Chem. Soc.*, 2014, **136**, 13154–13157.
36 Y. H. Kim, H. Cho, J. H. Heo, T. S. Kim, N. Myoung, C. L. Lee, S. H. Im and T. W. Lee, *Adv. Mater.*, 2015, **27**, 1248–1254.